Journal of Materials Science & Surface Engineering Vol. 4 (5), 2016, pp 415-424

Contents lists available at http://www.jmsse.org/

Journal of Materials Science & Surface Engineering

Silane-Coated Magnesium Implants with Improved *In-Vitro* Corrosion Resistance and Biocompatibility

Swati Gaur[1]*, Saumya Nigam[1], A.S.Khanna[2], R.K. Singh Raman[3]

[1]*IITB-Monash Research Academy, IIT Bombay, Powai, Mumbai 400076, India.*
[2]*Department of Metallurgical Engineering & Materials Science, IIT-Bombay, Powai, Mumbai 400076, India.*
[3]*Department of Mechanical and Aerospace Engineering, Monash University, Clayton, VIC-3168, Australia.*

Article history

Received: 18-July-2016
Revised: 27-July-2016
Available online: 21-Sep-2016

Keywords:
Corrosion,
Magnesium alloy,
Body implant,
Silanes,
Electrochemical impedance - spectroscopy,
Cytotoxicity

Abstract

Body implants, required to heal any impaired function like broken bones in the body, are either permanent, eg. Stainless steel implants or are temporary implants which need to be removed after healing of the bone. Alternately body implants using magnesium and its alloys though comes under temporary body implants but do not need 2nd surgery to remove as they degrade in the body itself slowly. Such Mg6ZnCa alloy appears to be a potential material in the category of temporary body implant applications which need to be removed through second surgery after healing of the bone takes place. However, a major challenge is the unacceptably high corrosion rate of magnesium that is not enough for the healing of bone. Its rapid dissolution due to corrosion in the body fluid needs modification to reduce its dissolution. Though, there are several engineering coatings used to reduce the corrosion rate of Mg and its alloys [1-5]. The present research, therefore, is to reduce this corrosion rate by developing coatings which are also compatible with body fluid. After a detailed literature survey, it was found that phosphate-silane coatings possess these properties [6-10]. Two types of phosphonato-silane coatings were developed which reduced the corrosion rate significantly, thereby providing a healing time from 10 h – 180 h [11, 12]. The present work demonstrates the use of combinations of Glycidoxypropyltrimethoxy-silane (GPTMS) with Methyltriethoxy-silane (MTEOS) based biocompatible protective coating that can further slow down the dissolution of a biodegradable magnesium alloy (Mg6ZnCa) in the early stages of healing and is also compatible to body fluid and enhance cells growth on the coated specimen.

GPTMS and MTEOS were mixed together in different molar ratios, namely, 1:1, 2:1 and 3:1 to form different coating systems and corrosion resistance of the coated alloy was characterized in modified simulated body fluid (*m*-SBF) using potentio-dynamic polarization and electrochemical impedance spectroscopy (EIS). The degradation of the coating over the time period, evaluated using EIS, suggests the coating's capability to resist corrosion at considerable rates by 280 h. From the morphological details, observed using SEM, it was found that as compared to bare Mg alloy, biological responses on the coated specimens, such as its tendency to attachment, viability, and differentiation of cells over a definite time period of 14 days was enhanced considerably, thus confirming, the improved activity of cell functions on this alloy with the sol–gel based silane coating treatment.

Abbreviations:

GPTMS	*Glycidoxypropyltrimethoxysilane*
MTEOS	*Methyltriethoxysilane*
m-SBF	*ModifiedSimulated body fluid*
HEPES	*2-(4-(2-hydroxyethyl)-1-piperazinyl) ethanesulfonic acid*
DMEM	*Dulbecco's Minimum Essential Medium*
PBS	*Phosphate Buffered Saline*
ALP	*Alkaline phosphatase*
EIS	*Electrochemical Impedance Spectroscopy*
EEC	*Electrical Equivalent Circuit*
CPE	*Constant Phase Element*
SEM	*Scanning Electron Microscopy*
ESEM	*Environmental Scanning Electron Microscopy*
EDX	*Energy Dispersive X-ray analysis*
FTIR	*Fourier Transform Infrared Spectroscopy*
XRD	*X-ray diffraction*

Introduction

Body implants are the essential requirement of several medical treatments, especially during bone healing due to fracture. Though the conventional materials such as stainless steels, titanium, Co-Cr alloys, are in use for a long time and are performing well, there is a serious limitation of these permanent implant materials. In use of such materials as temporary implants, there is a need for a second surgical procedure to remove the implant after the tissue has completely healed [13-15]. Medical fraternity was looking for a material which can bring some relief to the patients by way of avoiding the second surgery. This is where the alternative methodology of using biodegradable implants, becomes extremely attractive. The purpose of a temporary biodegradable implant is to support the healing of the tissues with material degradation and simultaneous its replacement through the surrounding tissues. Magnesium and its alloys have become an important tool of investigation in the hand of scientists due to its several excellent properties, such as light weight, good mechanical properties and ease of fabrication [16]. In order to search a suitable alloy for body implant, it must be assured that the alloy composition is non-toxic

Corresponding author. Tel.: +91-9987697502
E-mail address: gaurswat@gmail.com

and it has good compatibility with body fluid. Based upon several choices, Mg6ZnCa alloy was found to meet these requirements [14-15, 17-27]. However, this alloy also has quite high corrosion rate with concurrent high amounts of hydrogen gas formation that can delay the healing process. Biodegradable implants have controlled the rate of corrosion which can be achieved by modification of thealloy composition and/or the surface modification of the alloy to achieve the required corrosion resistance during the initial period where mechanical strength is required [22]. Retarding the rate of corrosion of Mg alloy is considered to be a more suitable strategy because a corrosion rate of Mg implant implies a decrease in the extent of alkalization and hydrogen evolution, which would facilitate the human body to gradually absorb or consume the corrosion products formed during magnesium degradation. Application of a corrosion resistant coating on magnesium alloy can delay the initiation of biodegradation and/or control or retard the degradation rate, allowing sufficient time for healing the fractured bone. Moreover, such coatings should be biocompatible and the corrosion products formed should be non- toxic [24-25, 28-30].

The present research, therefore, is to reduce this corrosion rate by developing coatings which are also compatible with body fluid. Two types of phosphonatosilane coatings were developed which reduced the corrosion rate significantly, thereby providing a healing time from 10 h – 180 h [11, 12]. In the present research, coatings based upon GPTMS and MTEOS were developed which brought down corrosion rate even further and provided healing duration up to 280 h. It is well known that GPTMS and MTEOS are among those silanes that possess characteristics that may be effective in both corrosion resistance and providing biocompatible surfaces [31-35]. MTEOS, when used for the formation of a sol-gel matrix, has hydrophobic property due to the methyl group that has a poor affinity for water, rendering the sol-gel surface hydrophobic [36]. GPTMS has been used to produce films with excellent biocompatibility in the field of tissue engineering scaffold [33]. The coatings were fully characterized for *in-vitro* corrosion and its compatibility with body fluid was studied using human osteoblast cells MG-63 to observe cell morphology, cell attachment, viability and differentiation on the bare and coated alloy specimens.

Therefore, the developed coating systems on the Mg6ZnCa alloy can find their use as bio-absorbable microclip, being used in endoscopic surgeries and wound closures where the existing devices resorb within 2 weeks. They can also be used as bio-absorbable surgical skin staples which are usually removed after 10-12 days of post-surgery. These coated magnesium alloy can also be used to replace Kirchner wires (K-wires) which are temporarily and frequently used for the stabilization of small fragments where healing is predictably quick. K-wires are used for temporary fixation during some operations and are usually removed 2-3 weeks post operation.

Experimental

Materials, reagents and corrosion test environment

The chemical composition of as-cast billet of Mg6ZnCa (wt %) alloy, used in this study is given in Table 1. GPTMS and MTEOS silane were procured from Sigma-Aldrich. Other chemicals (NaOH, glacial acetic acid and ethanol) were procured from Merck. Alloy test coupons (22x22x5 mm^3) were prepared using SiC papers up to 1500 grit and rinsed with deionized water and acetone. Metals and alloys generally require a surface pre-treatment for effective adherence of silanes [30]. The test coupons were pre-treated with NaOH following the optimized condition, as reported earlier [11], before application of the silane coating. The *in-vitro* corrosion test medium was modified simulated body fluid (*m*-SBF), maintained at 36.5 ± 0.5 °C throughout the test. The composition of *m*-SBF is given in Table 2. The solution was buffered with 2-(4-(2-hydroxyethyl)-1-piperazinyl) ethanesulfonic acid (HEPES) to simulate the physiological pH of 7.4 initially, which changes with time because of ongoing magnesium corrosion during immersion in *m*-SBF.

Table 1: Compositions of the alloy (wt %)

Alloy	Ca	Zn	Mg	Cu	Si	Fe	Ni
Mg6ZnCa	1	6	Bal	0.003	0.005	0.001	0.0005

Table 2: Composition of modified simulated body fluid (*m*-SBF)/liter [37]

Reagents	Amount
NaCl (g)	5.403
$NaHCO_3$ (g)	0.504
Na_2CO_3 (g)	0.426
KCl (g)	0.225
$K_2HPO_4.3H_2O$ (g)	0.23
$MgCl_2.6H_2O$ (g)	0.311
0.2M NaOH (ml)	100
HEPES (g)	17.892
$CaCl_2$ (g)	0.293
Na_2SO_4 (g)	0.072
1M NaOH (ml)	15

Coating procedure

GPTMS and MTEOS were mixed together in different molar ratios, namely, 1:1, 2:1 and 3:1. To this mixture, 0.05M acetic acid was added, which resulted in a silane-to-water weight % ratio of 15:85.The solution was aged in a closed container for three days under continuous stirring at ambient temperature[6]. The pre-treated specimens were immersed for 5–7 minutes in the silane solutions, and dried in air for 15 min. This was followed by curing at 120 °C for 1 h.

Corrosion evaluation

EIS and potentiodynamic polarization were performed on the bare and the coated specimens in the *m*-SBF medium using a Bio-logic SP-300 potentiostat, with a three-electrode system (specimens with an exposed area of 0.636 cm^2 as working electrode, a saturated calomel electrode (SCE) as the reference electrode and platinum was the counter electrode). The open circuit potential was monitored for 3500 s to confirm its stability at 10mV/sec. Potentiodynamic polarization tests were carried out, starting at 250 mV negative to the E_{corr} at a scan rate of 0.5 mV/s. A sinusoidal potential wave of amplitude 10 mV was applied at E_{corr} for EIS. The impedance response was measured over frequencies between 1 MHz and 10 mHz, recording 10 points per decade of frequency. The EIS data were analyzed using the ZsimpWin software. Each test was repeated thrice to examine the reproducibility of the results. A water bath with a submersible pump was used to simulate the *in-vitro* flow rate of the body fluid and the normal body temperature (36.5 ± 0.5 °C), respectively. A flow rate of 2.5 ml/ min was maintained [38-40].

A hydrogen evolution test was carried out by collecting the evolved H_2 in a measuring cylinder above the corroding specimens placed in *m*-SBF at 37 °C, as shown in Figure 1. The pH of the immersion solution was monitored every 24 h, using a pH meter (Model: sp-701; Suntex). The morphology and cross-section of the bare Mg alloy and coated specimens were examined using a scanning electron microscope (Model: Hitachi S-3400N). For examination of the cross section, the specimens were cold mounted edge-on, polished, and gold-coated prior to analysis. Fourier transform infrared spectroscopy (FTIR) (Bruker 3000 Hyperion Microscope with Vertex 80 FTIR System) was used to study the extent of crosslinking in the coating. XRD of the corroded specimen was done using X'Pert Pro Philips.

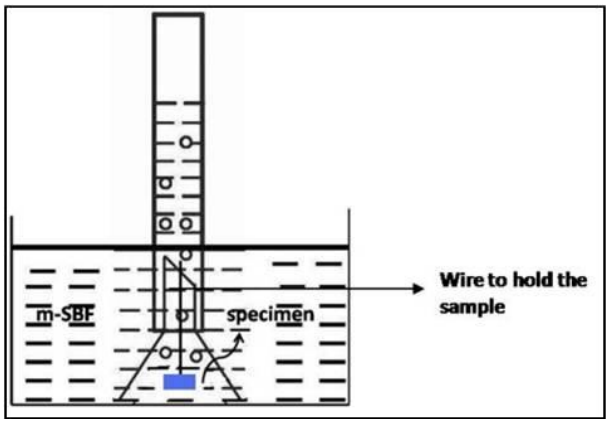

Figure 1: Schematic illustration of evolved hydrogen volume Measurement

Mechanical Properties of developed sol-gel coatings

Adhesion of the coating layer with the sample was assessed according to the ASTM D3359 standard test method using Cross Hatch Cutter. In this test, eleven cuts were made in two directions using the cutter at right angles to each other to form a grid of small squares. A pressure-sensitive adhesive tape was applied over the lattice and removed by pulling in a single smooth action. Adhesion was then assessed by comparing the fraction of coating removed from a grid of squares against the ASTM standard ratings. Hardness and scratch resistance of the coating were measured using Pencil Hardness Tester according to ASTM D 1522. The pencil hardness test is a constant-load scratch test. It uses pencil leads of different hardness grades as the scratch stylus. The hardest pencil grade that does not cause damage to the coated sample is considered as the pencil hardness of the coating.

***In-vitro* cell culture**

Cell culture

MG-63, a human-derived osteosarcoma cell line was cultured in DMEM supplemented with 10% fetal bovine serum and antibiotic/antimycotics at 37°C in a humidified 5% CO_2 environment. When cell culture flask was 85–90% confluent, the cells were treated with a trypsin-EDTA solution for detachment and counted under an optical microscope using a hemocytometer. For a typical experiment, cells with a typical count of 1×10^6 were seeded over the alloy specimen (exposed are: 1 × 1 cm^2), mounted over acrylic resin in a 35 mm sterile Petri dish in the supplemented tissue culture medium for 1, 3, 7, and 14 days at 37°C in a 5% CO_2 environment. The tissue culture media was replaced when exhausted. After the set intervals, the cells were harnessed from the alloy specimen and analyzed as described below. MG-63 cells, grown in Petri dish and those grown on the bare Mg6ZnCa alloy were considered as positive and negative controls respectively.

Cell morphology and attachment

After 1, 3, 7, and 14 days, the attached cells were observed by ESEM (Quanta 200FEG). Prior to the SEM observations, the media was removed from the Petri dish, the specimen was fixed with 3% glutaraldehyde for 5–6 h and incubated in a freshly prepared 1% carbohydrazide solution for 30 min. The specimen was then rinsed with PBS three to four times and sequentially dehydrated in graded ethanol (30, 50, 70, 90 and 100%) for 10 min each. The dehydrated specimen was vacuum dried and sputter-coated with platinum for observation under ESEM.

Cell viability and proliferation

Cell proliferation activity was evaluated using a Cyquant cell proliferation assay kit (C7026; Invitrogen) following the manufacturer's protocol. Toward the end of each time interval, the adhering cells were detached using a trypsin-EDTA solution and centrifuged to obtain a cell pellet. The cell pellet was suspended in the fluorescent dye solution that had the cell lysis buffer. The fluorescence of this lyzed cell pellet was recorded using a Thermo Scientific multiple plate reader (Thermo Varioskan Flash Multimode Reader)) at an excitation wavelength of 480 and emission wavelength of 520 nm. The measured fluorescence values were used to calculate the DNA content (expressed in µg/cell) against a DNA standard curve; R^2 = 0.997 (prepared as directed by manufacturer's manual). This fluorescence was also used to determine the percentage of the proliferation activity of the cells represented against the control cells according to the following equation;

$$\%\ Cell\ Proliferation = \frac{Flrs\ of\ cells\ from\ specimen\ harnessed\ at\ time\ 't'}{Flrs\ of\ control\ cells\ harnessed\ at\ time\ 't'} \times 100$$

Cell proliferation is directly proportional to the number of viable cells, and thus, a standard curve depicting a linear relation between cell number density and the fluorescence was made according to the manufacturer's manual (R^2 = 0.997).

Alkaline phosphatase activity assay

To evaluate cell differentiation, the activity of ALP as determined using colorimetric assay kit (Millipore, India) with minor modifications[41]. For ALP determination, the cells were washed with PBS and detached from the specimen and centrifuged to obtain a cell pellet. These cells were lyzed by 30% triton-X 100 and the lysate were put in a 96 well plate and mixed with 50 µl of a working assay solution. The plate was then incubated for 1 h at 37 °C in an incubator. After an hour, the 96-well plate was shaken for 2 min and the absorbance was measured at 570 nm (Thermo Scientific multi-well plate reader). The ALP activity was calculated against the standard plot, for the different time intervals. The standard plot depicted a linear behavior between the absorbance and the ALP activity from a known quantity of MG-63 cells (R^2 = 0.989).

Statistical analysis

The experimental results were represented as the mean value with a standard deviation of three independent experiments, performed at different times (n=3). Statistical analyzes were performed using the statistics functionality of Origin 9.1 software. A two-sample *t*-test was performed and the difference with $p< 0.05$ (*), $p<0.01$ (**) and $p< 0.001$ (***) was considered significantly different with an assumption of equal variance.

Results and Discussion

Surface characterization of silane-coated alloy

Fourier transform infrared spectroscopy (FTIR) of coating

The curing of the alkali-pre-treated silane-coated alloy was done at 120°C, and the extent of curing of silane coating developed with the different GPTMS:MTEOS volume ratios were examined by FTIR. For the coating, 790 cm^{-1} and 880 cm^{-1} peak correspond to Si-O-C (symmetric) and Si-OH respectively. The Si-OH peak intensity was maximum for the coating with 1:1 ratio that decreased considerably for 2:1 and was, in fact, absent for the coating with 3:1 ratio, indicating consumption of all Si-OH for the formation of Si-O-Si linkage in this case. The peak at 790 $cm^{-1}$was found to be absent in the cases of coatings with 2:1 and 3:1 ratios suggesting the conversion of Si-OEt to Si-OH and further Si-O-Si bond due to cross linking. The peak that appears at 1050 cm^{-1} in Figure 2, which corresponds to the asymmetric stretching of the Si-O-Si linkage, was observed in each case and confirms the

formation of a cross-linked siloxane network structure in the film. It is noted that the Si-O-Si band has a significantly lower intensity in the case of the coating with a 1:1 GPTMS:MTEOS, indicating a lesser extent of crosslinking as compared to the coating with the 3:1 ratio that showed maximum intensity for the Si-O-Si peak.

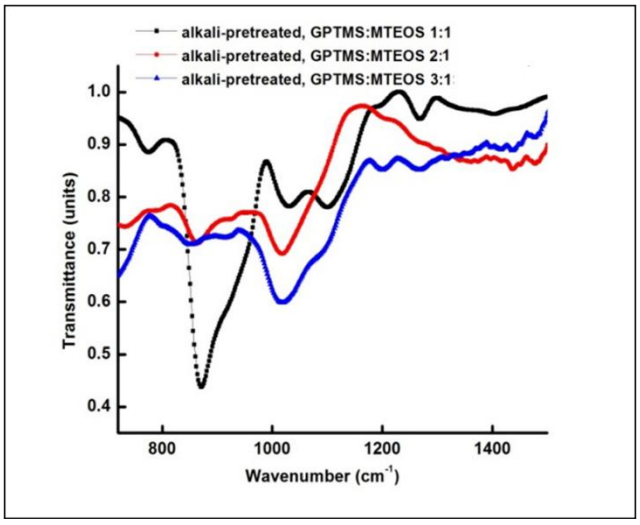

Figure 2: FTIR spectra of cured alkali-pre-treated alloy dipped in mixtures of silanes in different GPTMS:MTEOS volume ratios: (a) 1:1, (b) 2:1 and (c) 3:1

Morphology and chemical and mechanical properties of silane-coated alloy

Surface morphologies of the alloy coated with different mixtures of GPTMS:MTEOS molar ratios are shown in Figure 3. Specimen, coated with a GPTMS:MTEOS ratio of 3:1 was found to be the most defect-free (Figure 3c). EDX analysis of the coated alloy showed the presence of Si, Mg, Ca O, and carbon (Figure 3d). The thickness of this coating was found to be 21µm, as shown in Figure 4. The bonding strength was found by measuring the adhesion of the coatings to the substrate in accordance with ASTM D3359. The coatings showed strong adhesion with a rating of 5B; this rating corresponds to the best ASTM rating. Also, the pencil hardness of the coatings, as determined in accordance with ASTM D3363-92a, was found to be 4H. This adhesion value was same for all the mixing ratios of in the coating systems.

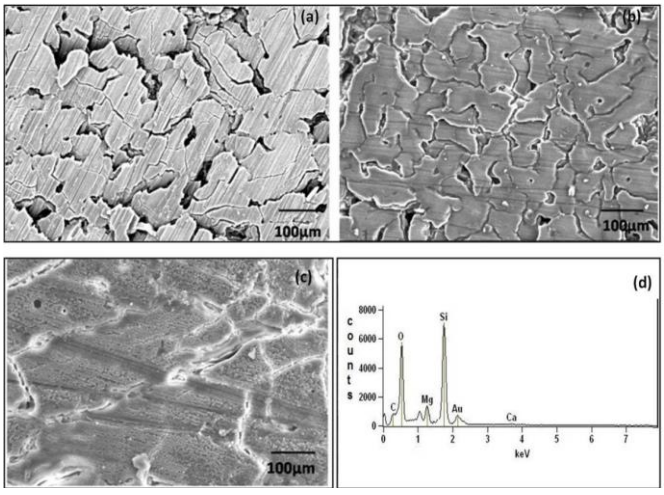

Figure 3: SEM micrographs of the surface morphology of alkali-pre-treated alloy dipped in mixtures of silanes in GPTMS:MTEOS volume ratios of: (a) 1:1, (b) 2:1, (c) 3:1and (d) EDX elemental analysis of 3:1 GPTMS:MTEOS-coated specimen

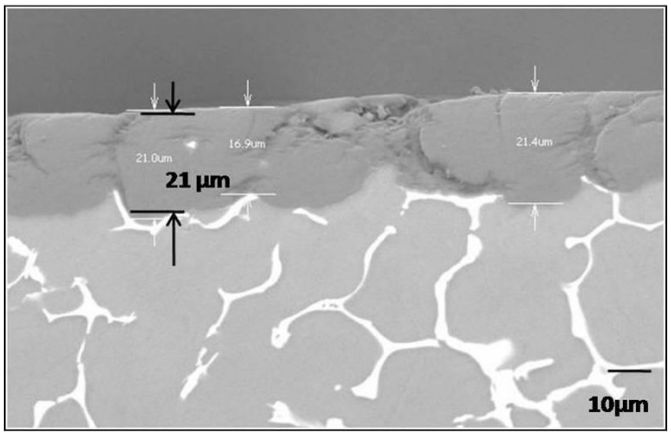

Figure 4: SEM micrographs of cross-sectional thickness of the coating with 3:1 GPTMS:MTEOS

Electrochemical investigation of GPTMS:MTEOS silane-coated alloy

Figure 5 shows the potentiodynamic polarization plots for the bare and GPTMS:MTEOS silane-coated specimens in *m*-SBF at 36.5 °C. The corrosion potential (E_{corr}) and the corrosion current density (i_{corr}), derived from these plots are presented in Table 3. The corrosion potential (E_{corr}) of the alloy coated with the 3:1 ratio was ~340 mV more noble when compared to the bare alloy. Also, the current densities in the anodic and cathodic parts of the polarization scans of the alloy with the 3:1 coating were two orders of magnitude lower when compared to the bare alloy (Table 3). The other two coatings with GPTMS:MTEOS ratios of 2:1 and 1:1 did not show significant improvement.

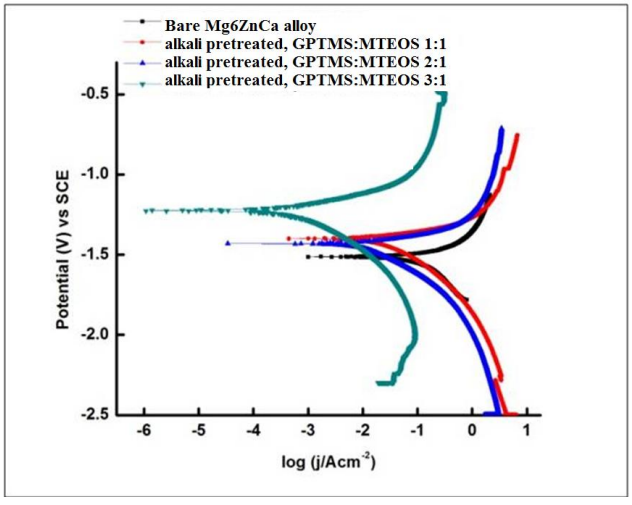

Figure 5: Potentiodynamic polarization in *m*-SBF at (36.5 ± 0.5) °C of the alloy coated with different GPTMS:MTEOS ratios of coating formulations

Table 3: Corrosion potential and corrosion current densities derived from plots in Figure 5

Specimens	E_{corr} (V)	i_{corr} (i/A cm^2)
Bare Mg6ZnCa alloy held in desiccator for 24 h	-1.57	1.58×10^{-1}
Alkali pre-treated, GPTMS: MTEOS 1:1	-1.40	7.42×10^{-1}
Alkali pre-treated, GPTMS: MTEOS 2:1	-1.43	1.44×10^{-2}
Alkali pre-treated, GPTMS: MTEOS 3:1	-1.23	2.85×10^{-3}

The EIS data for the bare and GPTMS:MTEOS-coated Mg6ZnCa alloy is shown in the form of Bode impedance plots in Figure 6. In a Bode impedance plot, the magnitude of impedance at the lowest frequency represents the polarization resistance. The impedance at the lowest frequency for all coated specimens

increased systematically with the change from 1:1 to 3:1in the GPTMS:MTEOS ratio in the coating formulation (Figure 6 and Table 4). The coating with GPTMS:MTEOS, 3:1 ratio provided an improvement in corrosion resistance of the bare Mg6ZnCa alloy by 5 orders of magnitude.

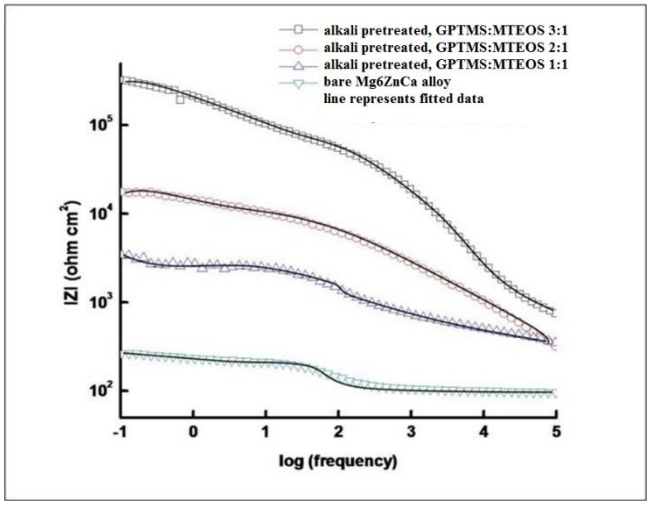

Figure 6: Bode plots in *m*-SBF at (36.5 ± 0.5) °C of the alloy coated with different GPTMS:MTEOS ratios of coating formulations.

Table 4: Impedance at the lowest frequency for the bare and coated alloys, derived from the plots in Figure 6

Specimens	Impedance $\|Z\|$(Ω cm^2)
Bare Mg6ZnCa alloy	$<10^2$
GPTMS: MTEOS 1:1	$5x10^3$
GPTMS: MTEOS 2:1	$2x10^4$
GPTMS: MTEOS 3:1	$4x10^5$

Time-dependent degradation of alloy with different GPTMS:MTEOS coatings

Coatings with each of the three GPTMS:MTEOS ratios resulted in a significant improvement in the corrosion resistance (impedance) of the alloy. Alloys with the three coatings were subjected to extended immersions in *m*-SBF, and the durability of corrosion resistance due to the coating was investigated after different durations of immersion. An EEC with three-time constants, as shown in Figure 7, was proposed for the GPTMS:MTEOS coated alloy to represent the interfaces: a substrate/surface hydroxide/*m*-SBF solution and a substrate/surface hydroxide/silane film/*m*-SBF solution. These interfaces are represented as a parallel combination of a capacitance and a resistance. In this EEC, Rs is the solution resistance and the silane-coated surface is represented by a parallel combination of the constant phase element CPE_f and resistance of the solution in the pores of that film R_f. The hydroxide layer is represented by C_{hyd} and resistance of the solution in the pores of hydroxide represented by R_{hyd}. The electrical double layer is represented as C_{dl} and a charge transfer resistance Rct.

As suggested by the Bode plots after different durations of immersion in *m*-SBF at (36.5 ± 0.5) °C(Figure 8), the coatings with the different ratios of GPTMS:MTEOS, showed reasonable corrosion resistance for different durations, namely, for 24 h for the ratio of 1:1(Figure 8a), 100 h for the ratio of 2:1(Figure 8b), and 280h for the ratio of 3:1 (Figure 8c).

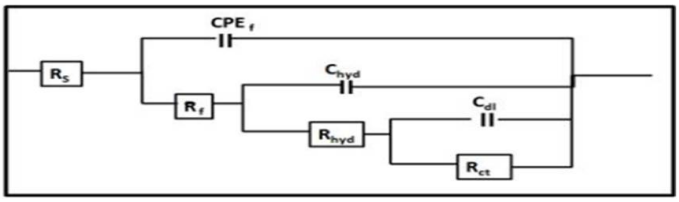

Figure 7: The electrical equivalent circuit that fits the experimentally obtained impedance data of specimen coated with a mixture of GPTMS:MTEOS

R_f is a measure of the resistance through the pores of the silane coatings and is inversely proportional to the extent and number of defects in the coating. The increase in R_f with the exposure time suggests the capacity of the coating to avoid pore formation. As is evident from Figure 8 and Table 7, a high R_f of the coating with the GPTMS:MTEOS ratio of 3:1is attributed to the highly cross-linked structure of this coating. The charge transfer resistance (Rct) is a measure of the corrosion process at the metal substrate underneath the coating. Rct decreases with time of immersion for all of the coatings. However, as shown in Tables 5-7, Rct after 2 h of immersion is considerably greater for the coating with a GPTMS:MTEOS ratio of 3:1 and it continues to be considerably greater after various immersion times. C_f and C_{hyd} indicate the physical properties of the coatings, such as thickness or water permeability. So, an increase in C_f and C_{hyd} with immersion time is attributed to the uptake of the electrolyte into the coating (Table 5-7). The increase in C_f and C_{hyd}, and the concurrent decrease in Rp (Table 5-7) represent the evolution of corrosion processes at the surface of the metal, and the degradation of the coating, such as its detachment the substrate.

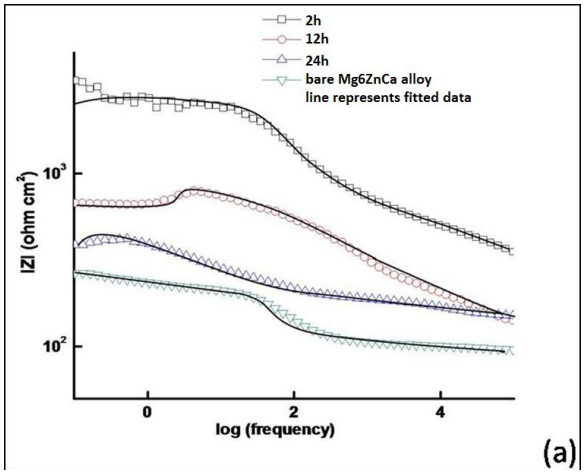

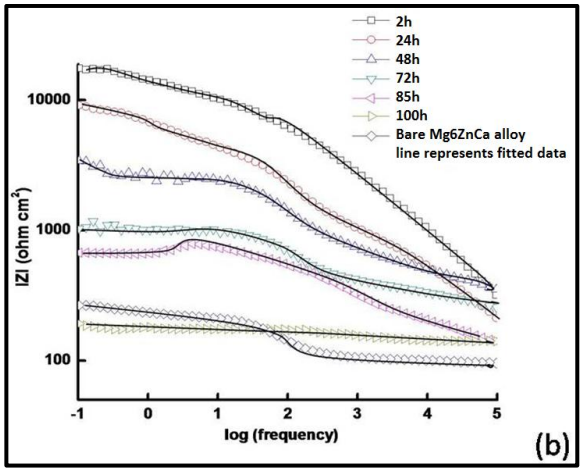

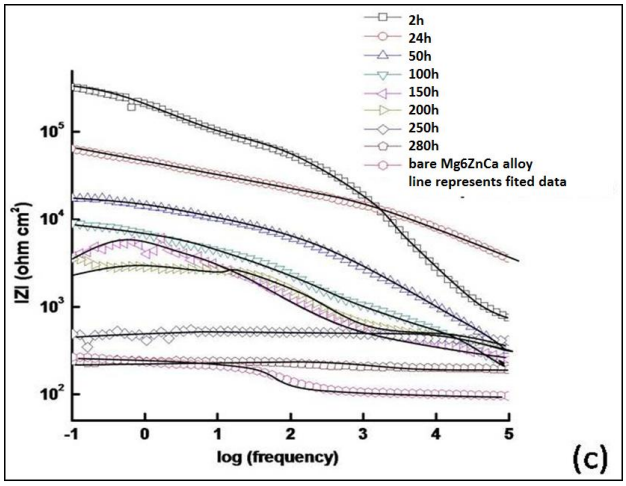

Figure 8: Bode plots of the alloy silane coated with (a) 1:1 GPTMS:MTEOS, after different durations of immersion in *m*-SBF at (36.5 ± 0.5) °C; (b) 2:1 GPTMS:MTEOS, after different durations of immersion in *m*-SBF at (36.5 ± 0.5) °C; (c) 3:1 GPTMS:MTEOS, after different durations of immersion in *m*-SBF at (36.5 ± 0.5) °C.

Table 5: Parameters calculated using EEC in Figure 8 for the alloy coated with the GPTMS:MTEOS in the ratio of 1:1, and then dipped in *m*-SBF at (36.5 ± 0.5) °C for different durations

Immersion Time [h]	R_f/[Ω cm^2]	CPE_f/[F cm^{-2}]	n	R_{hyd}/[Ω cm^2]	C_{hyd}/[F cm^{-2}]	C_{dl}/[F cm^{-2}]	R_{ct}/[Ω cm^2]	Rp/[Ω cm^2]
2	1765	$1.7x10^{-5}$	0.48	1535	$1.3x10^{-6}$	$3.6x10^{-5}$	1400	4700
12	283	$5.4x10^{-5}$	0.6	274	$2.5x10^{-5}$	$1.8x10^{-4}$	193	750
24	50.41	$4.1x10^{-5}$	0.63	168	$9.2x10^{-5}$	$2.7x10^{-4}$	102	320.41

Table 6: Parameters calculated using EEC in Figure 8 for the alloy coated with the GPTMS:MTEOS in the ratio of 2:1, and then dipped in *m*-SBF for different durations

Immersion Time [h]	R_f/[Ω cm^2]	CPE_f/[F cm^{-2}]	n	R_{hyd}/[Ω cm^2]	C_{hyd}/[F cm-^{2}]	C_{dl}/[F cm^{-2}]	R_{ct}/[Ω cm^2]	R_p/[Ω cm^2]
2	16079	$2.7x10^{-6}$	0.63	9178	$7.47x10^{-7}$	$1.7x10^{-5}$	7261	32458
24	4448	$1.2x10^{-5}$	0.42	2551	$4.5x10^{-6}$	$4.2x10^{-5}$	2776	9775
48	2436	$2.3x10^{-5}$	0.40	1987	$5.01x10^{-6}$	$4.8x10^{-5}$	1947	6370
72	408	$2.7x10^{-5}$	0.45	466	$2.1x10^{-5}$	$5.2x10^{-5}$	226	1100
85	351	$2.8x10^{-5}$	0.61	334	$7.3x10^{-5}$	$1.6x10^{-4}$	145	830
100	85	$10.1x10^{-5}$	0.63	156	$8.0x10^{-5}$	$2.8x10^{-4}$	99	340

Table 7: Parameters calculated using EEC in Figure 8 for the alloy coated with the GPTMS:MTEOS in the ratio of 3:1, and then dipped in *m*-SBF for different durations

Immer-sion Time [h]	R_f/[Ω cm^2]	CPE_f/[F cm^{-2}]	n	R_{hyd}/[Ω cm^2]	C_{hyd}/[F cm^{-2}]	C_{dl}/[F cm^{-2}]	R_{ct}/[Ω cm^2]	Rp/[Ω cm^2]
2	184679	$6.5x10^{-6}$	0.59	122256	$9.1x10^{-8}$	$8.5x10^{-6}$	78073	385008
24	36050	$1.2x10^{-5}$	0.44	22979	$4.5x10^{-7}$	$4.1x10^{-5}$	13246	72275
50	8636	$1.8x10^{-5}$	0.40	6787	$5.1x10^{-7}$	$4.9x10^{-5}$	4147	19570
100	3235	$2.7x10^{-5}$	0.48	2766	$2.1x10^{-6}$	$5.3x10^{-5}$	2599	8600
150	2181	$4.8x10^{-5}$	0.6	1464	$6.3x10^{-6}$	$6.3x10^{-5}$	1595	5240
200	850	$8.1x10^{-5}$	0.64	1268	$7.6x10^{-6}$	$7.2x10^{-5}$	997	3115
250	245	$9.1x10^{-5}$	0.67	200	$4.4x10^{-5}$	$8.3x10^{-4}$	267	712
280	85	$11.2x10^{-5}$	0.54	97	$6.5x10^{-5}$	$8.5x10^{-4}$	93	285

Hydrogen evolution and pH

Corrosion of magnesium and its alloys results in H_2 generation at a rapid rate ($Mg + 2H_2O = Mg^{2+} + 2OH^- + H_2$). H_2 bubbles can disrupt precipitation of bone-like apatite or bioactivity on the bone substrate. The application of an effective coating will decrease the corrosion rate as well as the concurrent H_2 generation and will thereby facilitate the *in-vitro* bioactivity. In this respect, it is important to assess the effectiveness of the coatings in retarding hydrogen evolution over extended exposure. According to the reaction, $Mg + 2H_2O=Mg^{2+}+2OH^- + H_2$; the evolution of one mole of hydrogen corresponds to the dissolution of one mole of magnesium. Thus, the estimation of the hydrogen generation rate is the direct measure of the magnesium dissolution rate. Using the set-up shown in Figure 1, triplicate runs were carried out to generate the hydrogen evolution rate data, while also examining the reproducibility of the data [42].

The evolved hydrogen was collected in a measuring cylinder that was placed above the corroding specimen, as shown in Figure 1. Coupons (surface area: 30 x 20 mm^2) of the bare Mg6ZnCa alloy and the GPTMS:MTEOS silane-coated samples were placed at the bottom of a 1000 ml beaker in a 500 ml solution of *m*-SBF at approximately 37°C for 320 h, and the volume of the evolved hydrogen was monitored as a function of immersion time.

As seen in Figure 9a, all the specimens exhibited an increase in the hydrogen evolution rate with increasing immersion time. The acceleration happened almost immediately in the case of the bare alloy, whereas, it was significantly delayed for the alloy with coatings with the different ratios of GPTMS:MTEOS. Consistent with the polarization and EIS data (Figure 5, 6 and 8), among the three coatings, the hydrogen evolution rate was the highest for the coating with 1:1 ratio of GPTMS:MTEOS and it was the lowest for coating with the ratio of 3:1.

The trend in the hydrogen evolution for the bare and coated alloy (Figure 9a) is also followed by the trend in the increase of pH (Figure 9b), which is understandable since the dissolution of magnesium also produces hydroxyl ions ($Mg + 2H_2O = Mg^{2+} + 2OH^- + H_2$.) High pH values are harmful to cell growth[24]. In this respect, it is noted that the pH of the test solution for the alloy with each of the coatings increased at a much slower rate than the bare alloy. However, what is most relevant is that the pH remained below 7.8 throughout the test duration (320 h), in the case of each of the coated alloys.

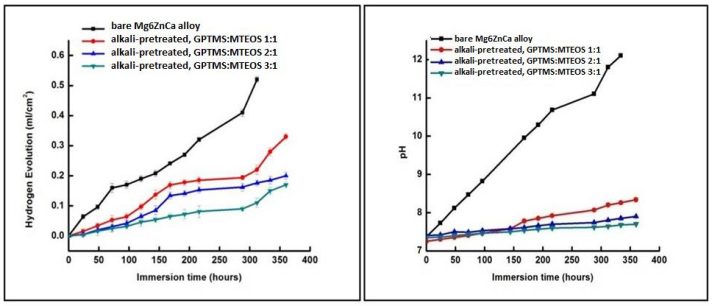

Figure 9: (a) Hydrogen evolution and (b) Variation of pH of bare and coated alloys, as a function of immersion time *m*-SBF at (36.5 ± 0.5) °C.

As established through electrochemical and immersion tests in *m*-SBF at (36.5 ± 0.5) °C, the silane coating with 3:1 ratio of GPTMS:MTEOS showed substantially superior corrosion resistance compared to coatings with other ratios (1:1 and 1:2). This trend is well supported by the FTIR and SEM results that established the maximum intensity for the peak representing crosslinking of Si-O-Si, and relatively lesser defects in the coating with the 3:1 ratio of GPTMS:MTEOS.

Post Corrosion Analysis

SEM image in Figure 10a shows the morphology of the alloy coated with the GPTMS:MTEOS, ratio of 3:1, after immersion in

m-SBF for 280 h. The micrograph shows a rough surface layer on the specimen with precipitates formed due to corrosion of the specimen in the *m*-SBF. EDX spectrum of this surface indicated the presence of Si, oxygen, magnesium, calcium, and zinc on the surface of the corroded specimen.

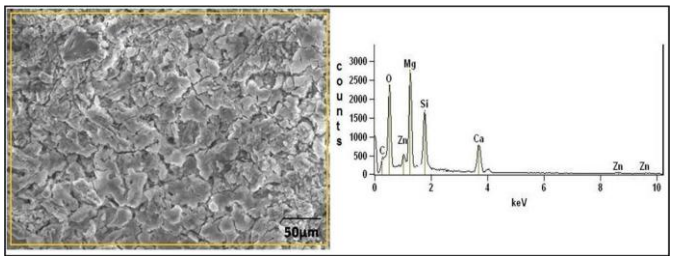

Figure 10: (a) SEM micrographs, (b) EDX of the alloy coated with 3:1 ratio of GPTMS:MTEOS, after immersion for 280 h in *m*-SBF at (36.5 ± 0.5) °C

These were further characterized by XRD. The XRD, as shown in Figure 11 suggest the formation of magnesium/calcium phosphate, along with magnesium hydroxide as per the following equation [43]:

$$Mg^{2+}\ (Ca^{2+}) + OH^{-} + HPO_4^{2-} + (n\text{-}1)\ H_2O \rightarrow Mg_x\ (or\ Ca)(PO_4)_y.n\ H_2O$$

This is an indication of a good bioactivity and osteo conductivity and is favourable to the increase in the chances for the formation of an osteointegrated interface after implantation. The presence of insoluble carbonates and phosphates on the magnesium alloy immersed in *m*-SBF had been reported by many studies[42-44].

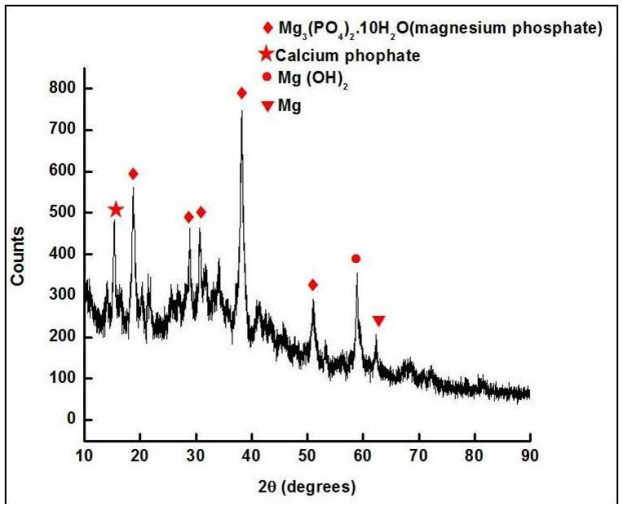

Figure 11: XRD spectra of the 3:1 GPTMS:MTEOS coated alloy after immersion for 280 h in *m*-SBF at (36.5 ± 0.5) °C

In-Vitro Cell Culture Studies

Cell morphology and attachment observations

The successful attachment of cells onto the surface of alloy specimen is a major characteristic in determining a favorable biological response toward the alloy implants. Figure 12 shows the electron micrographs depicting successful attachment and cell morphology of the MG-63 osteosarcoma cells on the surface of bare Mg6ZnCa and 3:1 GPTMS:MTEOS silane-coated Mg6ZnCa, after1, 3, 7, and 14 days. The positive control cells show normal morphology, and steady crowding of cells is observed over the experimental time period. The cell attachment on the surface of the bare Mg6ZnCa specimen shows strong differences from the first day of the study itself. It showed no cells or a very low number of cells attached to the surface, which further decreased over the fortnight due to the corrosion of the specimen resulting in hydrogen on the surface. The micrographs on day 3 and 7 show fewer cells that are also rounded-up, with the specimen that is primarily covered by the corrosion products. In contrast, the coated specimen shows initiation of attachment of cells on day 1 with spherical cellular morphology. By the end of day 3, these cells are seen to properly attach to the surface, and the cytoplasm of these cells is seen to be successfully spread, forming filopodia, and resulting in normal cellular morphology. By day 7, it was observed that the cells divided successfully since there was an increase in the number of viable cells. Also, the initiation of corrosion of the specimen could also be observed. The micrograph captured on day 14 of the study showed the formation of a thin cellular layer, covering the specimen along with the accumulation of corrosion products in the region. It can be seen that the cells are flattened and attached tightly to the coated surfaces with their filopodium. These results indicate the facilitation of the cell attachment on to the specimen by the coating, which delays the corrosion of the alloy and helps in improvement of the biological response toward the intended implant specimen.

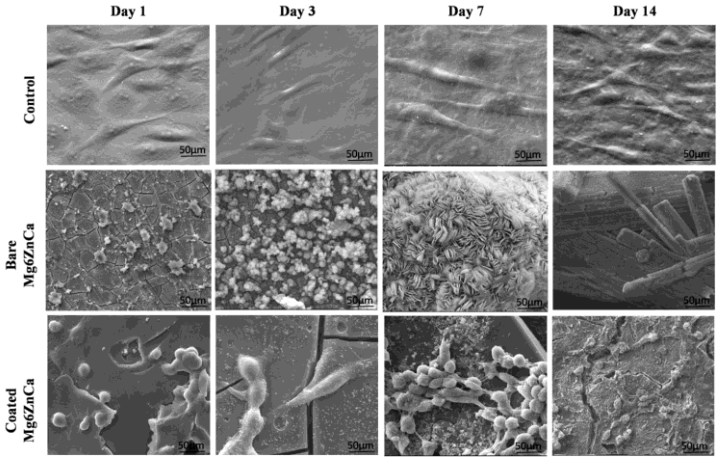

Figure 12: Electron micrographs depicting attachment of the MG-63 cells after culturing for 1, 3, 7, and 14 days on bare Mg6ZnCa and 3:1 GPTMS:MTEOS silane-coated Mg6ZnCa. The scale in the micrographs is of 50 µm

Cell viability and proliferation

Figure 13 (a) shows the percentage of cell proliferation represented against the proliferation of the positive control. It was observed that the cells proliferated better on the 3:1 GPTMS:MTEOS-coated Mg6ZnCa specimen as against the bare Mg6ZnCa sample ($p < 0.05$). The bare Mg6ZnCa specimen show a significant reduction in the cell proliferation activity of the MG-63 cells on and after three days of culturing. This reduction could largely be attributed to the sample undergoing corrosion and evolving hydrogen in the environment of the tissue culture medium, causing a severe increase in the pH of the culture medium. This increased alkalinity of the growth medium makes the environment unfavorable for cell growth and division and is largely responsible for the cell deaths that were present on the 1stday of the study. In contrast to the bare specimen, the coated alloy specimen was seen to support the cell proliferation over longer time durations and to an appreciable cell number density. The sol–gel based silane coatings hide the corrosive surface of the alloy and delay the specimen corrosion for considerable time duration. The water-based tissue culture medium is seen to initiate the degradation of this coating not before the seventh day of the experiment. The reduction in a cell population, seen on the day 7, and day 14, as compared to the day 3, is not much, which is in

agreement with the information obtained from the electron micrographs.

The quantification of DNA (µg/cell), was evaluated after the 1st, 3rd, 7th, and 14th day of culturing over the alloy specimens (Figure 13b), using the cell number density on the surfaces of specimens. The DNA content of MG-63 cells over the bare and silane-coated specimen was found to be in accordance with the cell proliferation activity. The viable cells present on the surface of these specimens are seen to be at their highest on the 1st day, decreasing significantly on the bare specimen; meanwhile, a gradual reduction of cell number was observed for the silane-coated specimen. The two sample *t*-test analysis of the difference of the population means were found to be significantly different at $p< 0.01$, while no significant difference was found at $p< 0.001$. In addition, at$p< 0.01$ the population variances were not significantly different.

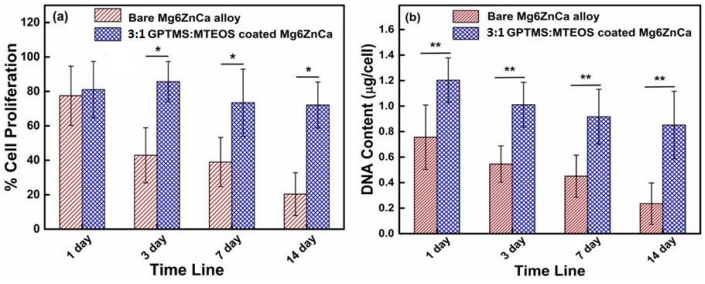

Figure 13: (a) Percentage cell proliferation observed on bare Mg6ZnCa and 3:1 GPTMS:MTEOS coated Mg6ZnCa calculated against positive control; at $p< 0.05$ level, the difference of means was found to be significantly different. (b) DNA content of MG-63 cells on the bare Mg6ZnCa and 3:1 GPTMS:MTEOS coated Mg6ZnCa; at $p< 0.01$ level, the difference of population means was found to be significantly different.

Alkaline phosphatase activity assay

Figure 14 shows the behavior of the ALP activity of MG-63 cells cultured over a period of 14 days. For cells cultured over the bare Mg6ZnCa specimen, moderate ALP activity was observed till day 3, which showed only a slight increase on day 7, while a negligible change was observed on day 14. In contrast, the cells cultured over the 3:1 GPTMS:MTEOS coated Mg6ZnCa specimen showed a moderate increase in ALP activity till the 3rd day of the study and substantially shot up on day 7, which reduced further on the 14th day of the study. The ALP activity of the cells on the coated samples showed higher expression levels compared to the bare Mg6ZnCa alloy. This higher ALP expression observed in the silane coating system confirms the enhancement of cell function and activity, at least at an early stage of differentiation[45].

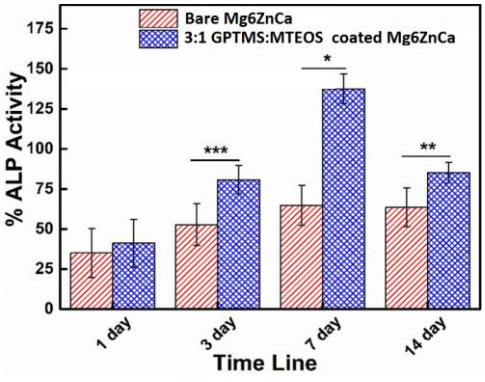

Figure 14: Percentage ALP activity of MG-63 cells cultured on bare Mg6ZnCa and 3:1GPTMS:MTEOS coated Mg6ZnCa calculated against ALP activity observed in positive control MG-63 cells; at p< 0.05, 0.01 and 0.001 level, the difference of means was found to be significantly different between bare Mg6ZnCa and 3:1 GPTMS:MTEOS coated Mg6ZnCa specimens

In spite of being a biologically active material, magnesium-based implants are highly susceptible to corrosion, which limits their promising implant application. A magnesium alloy when immersed in *m*-SBF at 37°C dissolves in aqueous environments by an electrochemical reaction, with the formation of magnesium hydroxide and hydrogen. However, the evolution of hydrogen and the associated pH changes are not desirable in biological situations. Both hydrogen and the pH increase can delay the growth of tissues and the healing process.

The purpose of the sol-gel based, cross-linked coatings of GPTMS and MTEOS, was to delay their rapid corrosion in the simulated physiological environment. The anodic dissolution rates of the silane-coated specimens were found to have slowed down because the coating blocks mass transport of Mg^{2+}. At the same time, the formation of Si-O-Mg bonds at the interface also blocks anodic reactions and retards the corrosion current. The shift of corrosion potential toward the cathodic direction also indicates that the hydrophobic silane film acts as a physical barrier to retard the electrolyte penetration, as observed from the potentiodynamic polarization study. Therefore, a significant delay in corrosion was achieved through a sol-gel based silane coating system with a considerable decrease in hydrogen evolution on the surface of the bare Mg6ZnCa alloy.

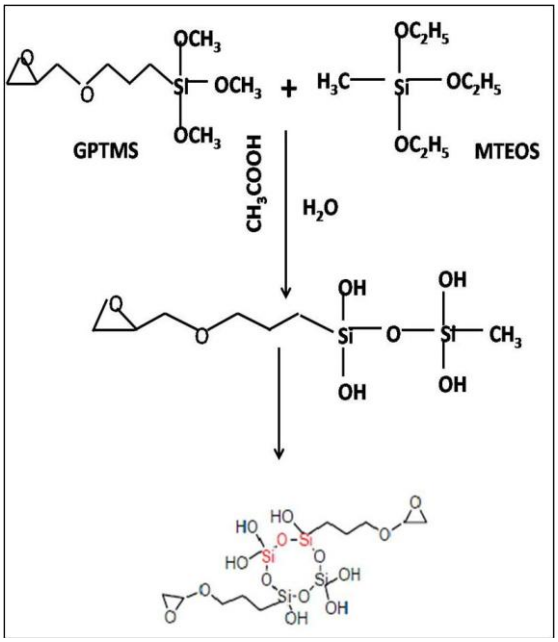

Figure15: Schematic representation of hydrolysis and condensation of GPTMS and MTEOS

The biological properties of the silane coating system were assessed in terms of their attachment, proliferation and differentiation behavior using MG-63 osteoblast cells. Local alkalization and hydrogen bubbles produce an unfavorable environment for the cells to attach. Therefore, only a few cells were detected on the bare Mg6ZnCa alloy samples. Since the 3:1 coated surface in *m*-SBF at (36.5 ± 0.5) °C also retarded hydrogen evolution and suppressed an increase in pH, it helped in the efficient attachment of cells. Therefore, good biocompatibility and favourable morphology of the GPTMS:MTEOS coated Mg6ZnCa alloy provided a suitable interaction environment, simultaneously enlarging the bioactive surface area as compared to bare alloy. The bioactive silane coated surface thereby supported the improved proliferation of cells and their further differentiation on the coated surface as compared to bare Mg6ZnCa alloy. The cells on the silane-coated Mg6ZnCa alloy specimen proliferated more actively and expressed ALP activity to a higher degree when compared to

those on the bare Mg6ZnCa alloy. This improved biocompatibility of the silane-coated alloy is due to the decreased surface reactivity of the coated alloy, thereby allowing the attachment, growth, and proliferation of the cells.The XRD analysis of the precipitated corrosion products formed on the surface of the silane coated alloys confirms the presence of calcium phosphates and magnesium phosphates that have been reported to enhance osteoblast activity and thereby accelerate bone growth.

Since, the silane-based coatings are water-based coatings and provide temporary barrier properties, they cannot protect metals indefinitely; when immersed continuously, the silane coatings hydrolyze and water eventually penetrates and reaches the interface. Since siloxane hydrolysis is a reversible process, the Si-O-Si bonds get converted back to Si-OH bonds, i.e. although corrosion inhibition of the metal is related to the formation of Mg—O—Si bond but this bond itself is not hydrolytically stable for longer immersion period. When exposed to a large amount of electrolyte, the Mg—O—Si bond is hydrolysed back to reform hydrophilic MgOH groups and SiOH groups. This, therefore, destroys the hydrophobicity of the metal surface after exposure to the electrolyte for a longer period of time. Therefore, the improvement achieved in this study may be sufficient for implants required for short-term applications; it may be inadequate for a longer service life. This insufficiency of the coating can also be attributed to the presence of inherent intermetallics on the magnesium alloy surface, which interfered with the development of a robust hydroxide surface, and a much more corrosion-resistant coating on top, unlike what was expected. This led to micropores, cracks and areas with low cross-link density. These areas facilitate the diffusion of aggressive electrolytes to the coating/substrate interface and provide preferential sites for corrosion initiation.

Conclusions

A protective silane coating that was developed using a mixture of GPTMS and MTEOS silanes was deposited onto Mg6ZnCa alloy specimen, using the sol-gel technique. A comparative study of the corrosion resistance offered by the silane-coated alloy and the uncoated Mg6ZnCa alloy suggests that the rate of corrosion reduces substantially for the coated alloy compared to the bare alloy. The current density of the formulation with the 3:1 molar ratio of GPTMS:MTEOS was found to be approximately two orders of magnitude lower than that of the substrate. The degradation of the coating over the time period, evaluated using EIS, suggests the coating's capability to resist corrosion at considerable rates by 280 h. A significant decrease in hydrogen evolution and a lesser increase in pH, which is both desirable for the use of magnesium alloys as implants, was also achieved. Magnesium and calcium phosphate along with magnesium hydroxide that was formed as corrosion products have been reported to be biologically active and support the osteoblast formation. The *in vitro* cell culture results clearly indicate the superiority of the silane-coated Mg6ZnCa alloy, which significantly contributes to the improvement of corrosion resistance and interactions between surfaces of the implanted specimen and the cell membrane. The sol-gel coatings developed for the Mg6ZnCa alloy, therefore, promise a controlled dissolution of the body implant, as may be required for a particular application such as bio-absorbable surgical skin staples (needs to be removed after 10-12 days of post-surgery), micro-clips (needs to degrade within 2 weeks) and pins used in fingers dislocation or fracture which are predicted to heal quickly.

Acknowledgements

I thank Department of Metallurgical Engineering and Materials Science for SEM and SAIF IIT Bombay for FTIR and ESEM analysis facilities.

Conflict of Interest: The authors declare that they have no conflict of interest.

References

1. Al-Abdullat, Y., et al., Surface modification of magnesium by NaHCO3 and corrosion behavior in Hank's solution for new biomaterial applications. MATERIALS TRANSACTIONS. 42(8): p. 1777 - 1780.
2. Chiu, K.Y., et al., Characterization and corrosion studies of fluoride conversion coating on degradable Mg implants. Surface and Coatings Technology, 2007. 202(3): p. 590-598.
3. Xu, L., E. Zhang, and K. Yang, Phosphating treatment and corrosion properties of Mg–Mn–Zn alloy for biomedical application. Journal of Materials Science: Materials in Medicine, 2009. 20(4): p. 859-867.
4. Yang, J., F. Cui, and I.S. Lee, Surface modifications of magnesium alloys for biomedical applications. Ann Biomed Eng, 2011. 39(7): p. 1857-1871.
5. Zomorodian, A., et al., Anti-corrosion performance of a new silane coating for corrosion protection of AZ31 magnesium alloy in Hank's solution. Surface and Coatings Technology, 2012. 206(21): p. 4368-4375.
6. Khramov, A.N., et al., Nanostructured sol–gel derived conversion coatings based on epoxy- and amino-silanes. Progress in Organic Coatings, 2003. 47(3–4): p. 207-213.
7. Khramov, A.N. and J.A. Johnson, Phosphonate-functionalized ORMOSIL coatings for magnesium alloys. Progress in Organic Coatings, 2009. 65(3): p. 381-385.
8. Kirchner, C., et al., Cytotoxicity of Colloidal CdSe and CdSe/ZnS Nanoparticles. Nano Letters, 2004. 5(2): p. 331-338.
9. Kotov, N.A., et al., Nanomaterials for Neural Interfaces. Advanced Materials, 2009. 21(40): p. 3970-4004.
10. Ying, J., N. Jana, and Y. Zheng, Water-Soluble, surface-functionalized nanoparticle for bioconjugation via universal silane coupling, 2006, WO Patent 2,006,080,895.
11. Gaur, S., R.K. Singh Raman, and A.S. Khanna, In vitro investigation of biodegradable polymeric coating for corrosion resistance of Mg-6Zn-Ca alloy in simulated body fluid. Materials Science and Engineering: C, 2014. 42(0): p. 91-101.
12. al, S.G.e., In-vitro evaluation of degradation of biodegradable silane based coating on Mg-Zn-Ca alloy in a physiological environment. Materials Science Forum, 2013. 765: p. 803-807.
13. Manivasagam, G., D. Dhinasekaran, and A. Rajamanickam, Biomedical implants: Corrosion and its prevention-a review. Recent Patents on Corrosion Science, 2010. 2(1): p. 40-54.
14. Shaw, B.A., E. Sikora, and S. Virtanen, Fix, heal, and disappear: A new approach to using metals in the human body. The Electrochemical Society Interface, 2008. 17(2): p. 45.
15. Staiger, M.P., et al., Magnesium and its alloys as orthopedic biomaterials: A review. Biomaterials, 2006. 27(9): p. 1728-1734.
16. Brar, H., et al., Magnesium as a biodegradable and bioabsorbable material for medical implants. JOM, 2009. 61(9): p. 31-34.
17. Avedesian, M.M., H. Baker and A.S.M.I.H Committee, Magnesium and Magnesium alloys, 1999, ASM International: Materials park, OH:.
18. Gu, X.-N. and Y.-F. Zheng, A review on magnesium alloys as biodegradable materials. Frontiers of Materials Science in China, 2010. 4(2): p. 111-115.
19. Li, Z., et al., The development of binary Mg–Ca alloys for use as biodegradable materials within bone. Biomaterials, 2008. 29(10): p. 1329-1344.
20. Choudhary, L., R.K.S. Raman, and J.F. Nie, In Vitro Evaluation of Degradation of a Calcium Phosphate Coating on a Mg-Zn-Ca Alloy in a Physiological Environment. Corrosion, 2012. 68(6): p. 499-506.
21. Choudhary, L. and R.K. Singh Raman, Magnesium alloys as body implants: Fracture mechanism under dynamic and static loadings in a physiological environment. Acta Biomater, 2012. 8(2): p. 916-923.
22. Kannan, M.B. and R.K.S. Raman, In vitro degradation and mechanical integrity of calcium-containing magnesium alloys in modified-simulated body fluid. Biomaterials, 2008. 29(15): p. 2306-2314.

23. Seal, C.K., K. Vince, and M.A. Hodgson, Biodegradable surgical implants based on magnesium alloys – A review of current research. IOP Conference Series: Materials Science and Engineering, 2009. 4(1): p. 012011.
24. Song, G., Control of biodegradation of biocompatable magnesium alloys. Corrosion Science, 2007. 49(4): p. 1696-1701.
25. Song, G. and S. Song, A Possible Biodegradable Magnesium Implant Material. Advanced Engineering Materials, 2007. 9(4): p. 298-302.
26. Witte, F., The history of biodegradable magnesium implants: A review. Acta Biomater, 2010. 6(5): p. 1680-1692.
27. Wolf, F.I. and A. Cittadini, Chemistry and biochemistry of magnesium. Molecular Aspects of Medicine, 2003. 24(1–3): p. 3-9.
28. Hornberger, H., S. Virtanen, and A.R. Boccaccini, Biomedical coatings on magnesium alloys – A review. Acta Biomater, 2012. 8(7): p. 2442-2455.
29. Zomorodian, A., et al., Corrosion resistance of a composite polymeric coating applied on biodegradable AZ31 magnesium alloy. Acta Biomaterialia, 2013. 9(10): p. 8660-8670.
30. Zomorodian, A., et al., Biofunctional composite coating architectures based on polycaprolactone and nanohydroxyapatite for controlled corrosion activity and enhanced biocompatibility of magnesium AZ31 alloy. Materials Science and Engineering: C, 2015. 48: p. 434-443.
31. Ballarre, J., et al., Improving the osteointegration and bone-implant interface by incorporation of bioactive particles in sol-gel coatings of stainless steel implants. Acta Biomater, 2010. 6(4): p. 1601-9.
32. Bariana, M., et al., Tuning drug loading and release properties of diatom silica microparticles by surface modifications. International Journal of Pharmaceutics, 2013. 443(1–2): p. 230-241.
33. Guo, R., et al., Bioadhesive film formed from a novel organic–inorganic hybrid gel for transdermal drug delivery system. European Journal of Pharmaceutics and Biopharmaceutics, 2011. 79(3): p. 574-583.
34. Pathak, S.S. and A.S. Khanna, Synthesis and performance evaluation of environmentally compliant epoxysilane coatings for aluminum alloy. Progress in Organic Coatings, 2008. 62(4): p. 409-416.
35. Pathak, S.S., A.S. Khanna, and T.J.M. Sinha, HMMM cured corrosion resistance waterborne ormosil coating for aluminum alloy. Progress in Organic Coatings, 2007. 60(3): p. 211-218.
36. McDonagh, C., B.D. MacCraith, and A.K. McEvoy, Tailoring of Sol−Gel Films for Optical Sensing of Oxygen in Gas and Aqueous Phase. Analytical Chemistry, 1998. 70(1): p. 45-50.
37. Oyane, A., et al., Preparation and assessment of revised simulated body fluids. J Biomed Mater Res A, 2003. 65(2): p. 188-95.
38. Kang, Y., et al., A comparative study of the in vitro degradation of poly(l-lactic acid)/β-tricalcium phosphate scaffold in static and dynamic simulated body fluid. European Polymer Journal, 2007. 43(5): p. 1768-1778.
39. Duan, Y., et al., [Effects of simulated body fluid flowing rate on bone-like apatite formation on porous calcium phosphate ceramics]. Hang tian yi xue yu yi xue gong cheng= Space medicine & medical engineering, 2002. 15(3): p. 203-207.
40. Duan, Y., et al., Dynamic study of calcium phosphate formation on porous HA/TCP ceramics. Journal of Materials Science: Materials in Medicine, 2005. 16(9): p. 795-801.
41. Zhao, S.-f., et al., Effects of magnesium-substituted nanohydroxyapatite coating on implant osseointegration. Clinical Oral Implants Research, 2013. 24: p. 34-41.
42. Xin, Y., T. Hu, and P.K. Chu, Degradation behaviour of pure magnesium in simulated body fluids with different concentrations of. Corrosion Science, 2011. 53(4): p. 1522-1528.
43. Lorenz, C., et al., Effect of surface pre-treatments on biocompatibility of magnesium. Acta Biomater, 2009. 5(7): p. 2783-2789.
44. Xin, Y., et al., Corrosion behavior of biomedical AZ91 magnesium alloy in simulated body fluids. Journal of materials research, 2007. 22(07): p. 2004-2011.
45. Ali, N.N., J. Rowe, and N.M. Teich, Constitutive expression of non-bone/liver/kidney alkaline phosphatase in human osteosarcoma cell lines. Journal of Bone and Mineral Research, 1996. 11(4): p. 512-520.